We would like to thank the Editor and the two Referees for the additional comments. Referee comments from the Editor report are shown below with italicized font and our replies including the updates to the manuscript are shown after each comment. A marked-up manuscript version is also showing the updates.

Referee #1:

The paper has been largely improved but these points are still not resolved. It may be published after these are considered.

1. You have done the back trajectory analysis however have not found anything interesting, which means the sources are more local or basically very mixed? Could we get a general idea how much BC could be from biomass burning or traffic? I can marginally see the phase transition from the shift of BC features, is it at least associated with air mass coming from easterly or westerly?

Our back trajectory analysis showed that most trajectories are originating from North West sector not far from the measurement sites. This means that the air masses are well mixed, but it cannot rule out local emissions. Since there is nothing new in this, we have left out the trajectory analysis. We were not able to separate particles from biomass burning and traffic. We are not sure what the Referee means by "the phase transition from the shift of BC features". For us the only statistically clear feature is the diurnal cycle.

2. Is the very large BC maybe because of the dust? The GMD for Gual looks too large to me.

We have examined single particle signals, but did not see any evidence of dust (e.g. clear differences in wide band to narrow band incandescence ratios). This is already mentioned in the manuscript. Gual Pahari GMD is larger due to the larger fraction of large rBC particles. Also note that volume mean diameter is larger than number mean diameter.

3. It is better to use image plot for Fig. 7. and with colour scaled legend. It looks the bottom panel also has the second mode just been hidden by the other too populated mode.

We ended up using a linear grayscale, because we wanted to show the relevant importance of the different modes, which is in line with reporting average values. A non-linear color scale could highlight the second mode in the bottom panel, but these are a small fraction of all particles and therefore are not that important for the averages. A legend has been added. For that we have normalized the data so that both cover the same range (from 0 to 1). Changes to the text and Fig. 7 are shown below.

Page 10, lines 4-6: "Figure 7 shows the dependency of the optical size on the rBC core size by means of a normalized probability density map (normalized by the maximum probability density)~~(darker color means higher probability)~~."

Figure 7, caption: "Distributions of single particle optical and rBC core diameters for the 360 nm mobility size and 30–35 °C instrument temperature range (probabilities normalized by the maximum values)~~(darker color indicates higher probability)~~."

Figure 7, original (left) and updated (right):

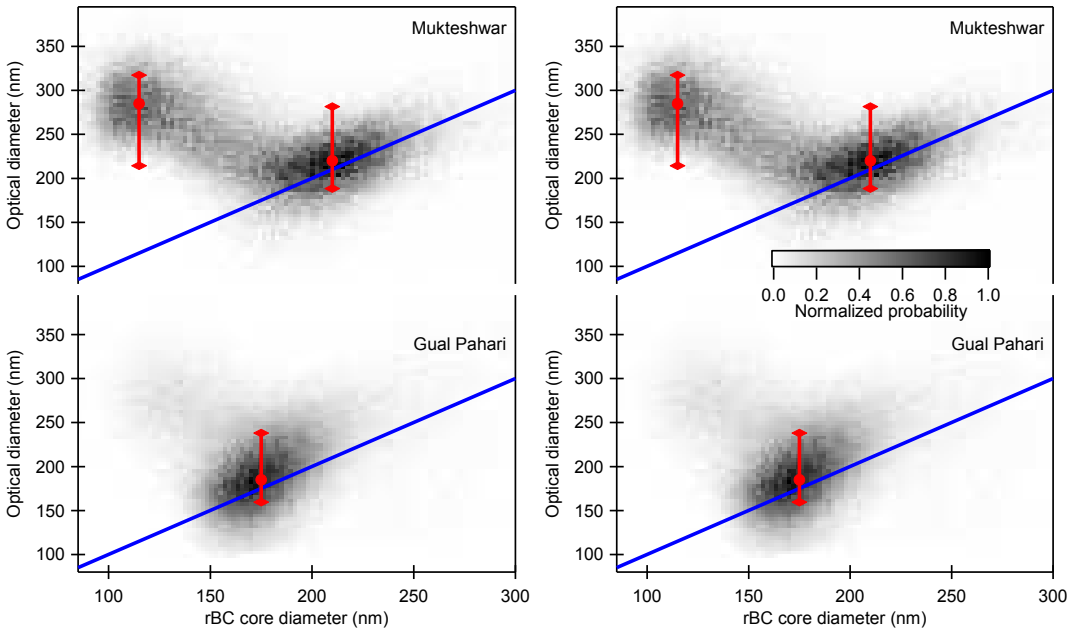

4. Regarding the optical/mobility diameter of BC and BC core, could we have more details about Dm vs Do. The Dc/Dm tells the mixing state and Dm/Do tells the morphology.

We are unsure of what kind of details would be needed, but there is not much more that could be provided. Time series, for example, are incomplete due to the problems with the LEO method at instrument temperatures below 30 °C. Also, we are not showing size-resolved LEO results, because optical sizes have a narrow sizing range (the detection limit is about 200 and the calibration extends up to about 450 nm) compared with that of the rBC cores.

5. The bottom line of this paper is still not very conclusive, for example, you could have answered the questions: why distinct features of BC from two places, in terms of BC mixing state, size, and morphology. It's not really getting the punching point yet.

We have used this data to show the distinct features of rBC from two places, but the data itself does not explain why they are distinct. In the absence of additional data that could link our observations to the sources and because trajectories could not provide this information, we have given up from the source analysis.

Referee #2:

The authors have addressed most of the reviewer comments adequately, and the organization and presentation of the results is much clearer in the revised version. I would feel more confident in recommending publication if the authors were able to find the causes of several somewhat odd features of the data, such as the SP2 over counting and the temperature dependences. They are, however, quite transparent in the treatment of these issues, and the rarity of data in this region coupled with the interesting DMA -> SP2 are both strengths

We have spent a lot of time in finding an explanation for the SP2 over counting and the temperature dependences. We have also made some experiments to quantify their effects (unpublished results), but we just don't have solid explanations for the causes. Nevertheless, the temperature dependency is a known issue and the over counting is a known issue for our SP2 that was used in the India measurements. Even if we could not confirm causes for these, we will clarify that these are known issues and there is a simple correction to the over counting and the weak temperature dependency is not a significant problem especially when we are focused on the rBC size.

Update in page 4, lines 23-25: "Consistency tests showed that the SP2 over counted particles compared with the parallel CPC measurements, which is a known issue for this specific SP2 (Supplementary Material). Multiplying all SP2 concentrations by a factor of 0.82 made the SP2 and CPC number concentrations levels similar with just noise-like variability. Consistency tests also showed that the DMA-selected mobility sizes are in good agreement with those measured by the SP2 (particles without rBC) although a weak dependency on the SP2 temperature was observed (known issue for all SP2s)."

Size-selected black carbon mass distributions and mixing state in polluted and clean environments of northern India

Tomi Raatikainen[1], David Brus[1], Rakesh K. Hooda[1,2], Antti-Pekka Hyvärinen[1], Eija Asmi[1], Ved P. Sharma[2], Antti Arola[3], and Heikki Lihavainen[1]

[1]Finnish Meteorological Institute, Helsinki, Finland
[2]The Energy and Resources Institute, Delhi, India
[3]Finnish Meteorological Institute, Kuopio, Finland

Correspondence to: T. Raatikainen (tomi.raatikainen@fmi.fi)

Abstract. We have measured black carbon properties by using a size-selected Single Particle Soot Photometer (SP2). The measurements were conducted in northern India at two sites: Gual Pahari is located at the Indo-Gangetic plains (IGP) and Mukteshwar at the Himalayan foothills. Northern India is known as one of the absorbing aerosol hot spots, but detailed information about absorbing aerosol mixing state is still largely missing. Previous equivalent black carbon (eBC) mass concentration measurements are available for this region and these are consistent with our observations showing that refractory black carbon (rBC) concentrations are about ten times higher in Gual Pahari than those at Mukteshwar. Also the number fraction of rBC-containing particles is higher in Gual Pahari, but individual rBC-containing particles and their size distributions are fairly similar. These findings indicate that particles at both sites have similar local and regional emission sources, but aerosols are also transported from the main source regions (IGP) to the less polluted regions (Himalayan foothills). Detailed examination of the rBC-containing particle properties revealed that they are most likely irregular particles such as fractal aggregates, but the exact structure remains unknown.

1 Introduction

Absorbing aerosols are warming the global climate, but uncertainties are still significant partly due to the lack of detailed experimental data on aerosol spatial and temporal distributions and their physical properties (Stocker et al., 2013; Bond et al., 2013). Broadly defined black carbon (BC) is typically the main absorbing aerosol component in submicron aerosols and its radiative effects depend on absolute concentrations and mixing state, which describes how BC is distributed within the aerosol particles (Bond and Bergstrom, 2006; Petzold et al., 2013; Lack et al., 2014). Although BC mass concentrations are often measured, the information about the mixing state is currently limited. For some sources the freshly emitted BC can be almost pure black carbon, but rapid atmospheric processing leads to mixed particles containing significant mass fractions of other typical aerosol species such as sulphate and organics. The inclusion of non-absorbing components may cause an increase to BC absorption by a so-called lensing effect, but this also depends on the structure of the particle (e.g., Adachi et al., 2010; Cappa et al., 2012; He et al., 2015; Peng et al., 2016). In addition to the direct radiative effect, aerosol water uptake depends on the volume fraction of soluble aerosol species as pure BC is hydrophobic. Some absorbing aerosol particles can act as a

cloud condensation nuclei (CCN), which means that BC can have an effect on cloud properties (an indirect climate effect). Therefore, knowing the mixing state is highly important when assessing the climate effects of BC.

Recent development of single particle instruments capable of detecting BC (e.g., Cross et al., 2010; Lack et al., 2014) has provided detailed information about the BC mixing state. One widely used instrument for this purpose is the Single Particle Soot Photometer, SP2, (Stephens et al., 2003; Schwarz et al., 2006; Moteki and Kondo, 2007) developed by Droplet Measurement Technologies (Boulder, CO, USA). This instrument uses laser induced incandescence technique to detect so-called refractory black carbon (rBC), which is the fraction of the absorbing carbonaceous material that has boiling point close to 4000 K and emits visible light when heated to that temperature (Petzold et al., 2013; Lack et al., 2014). The rBC mass can be detected accurately for most particle types (e.g., Slowik et al., 2007; Cross et al., 2010), while determining the size of the particle containing both rBC and non-refractory material requires significant assumptions about the particle properties (e.g., Taylor et al., 2015). These uncertainties dealing with determining the particle sizes are further reflected in calculations of mixing state parameters such as the rBC volume fraction in each particle and the number fraction of rBC-containing particles.

Due to the significant local and regional emissions and prevailing meteorological conditions, northern India is one of the global absorbing aerosol hot spots (Ramanathan et al., 2007). The low frequency of rainfall during the winter and spring months allows the accumulation of aerosol pollutions, which can be observed as a brown cloud (Ramanathan et al., 2001, 2007). Although the absorbing dust aerosol is mainly from natural origin, anthropogenic emissions such as biofuel burning and road traffic produce large amounts of black carbon. Aerosol concentrations are decreased significantly when the monsoon rains arrive (typically between mid-June and July in northern India). However, it has been suspected that the increased aerosol absorption could have an effect on the monsoon (e.g., Menon et al., 2002; Bollasina et al., 2008, 2011; Gautam et al., 2009; Lau et al., 2010; Ganguly et al., 2012; D'Errico et al., 2015; Boos and Storelvmo, 2016), which has a great importance for the whole south Asia. In spite of the potential importance of the absorbing aerosol, there has been little published information about the BC mixing state in India.

The main purpose of this study is to provide new and detailed information about the rBC mixing state in northern India focusing on two different environments: polluted Indo-Gangetic plains and relatively clean Himalayan foothills. Comparing these observations gives us additional experimental information about processes affecting on the transport and uplift of absorbing aerosol from the plains towards Himalayan foothills. Observations are made with a new measurement system where Differential Mobility Analyzer (DMA) is used to size-select ambient particles before measuring rBC properties with a Single Particle Soot Photometer (SP2). This system provides size-resolved information about rBC mixing state parameters including rBC number fractions and rBC mass in each particle. Also, comparing the DMA-selected particle size with that measured by the SP2 gives additional information about particle morphology.

2 Methods

2.1 Measurement sites

Mixing state of the rBC aerosol was measured in northern India in Mukteshwar, Nainital (29.47° N, 79.65° E, 2180 m above sea level) and Gual Pahari, Gurgaon (28.43° N, 77.15° E, 243 m above sea level) during the spring and pre-monsoon season 2014. Figure 1 shows the station locations. The measurements were started in Mukteshwar (9.2.-31.3.2014) and then the instruments were moved to Gual Pahari (3.4.-14.5.2014). Mukteshwar is a relatively clean site at the foothills of the central Himalayas about 2 km above the Indo-Gangetic plains (IGP) and Gual Pahari station is located at the plains close to Delhi where aerosol concentrations are significantly higher (e.g., Hyvärinen et al., 2009, 2010; Komppula et al., 2009; Panwar et al., 2013; Raatikainen et al., 2014; Hooda et al., 2016).

2.1.1 Measurement setup

Refractory black carbon (rBC) concentrations and mixing state parameters were measured by a Single Particle Soot Photometer (SP2; Revision C* with 8 channels), manufactured by the Droplet Measurement Technologies (Boulder, CO, USA), which was connected to a Differential Mobility Particle Sizer (DMPS). Details of the DMPS-SP2 measurement setup, data analysis and a series of consistency tests are given in the Supplementary Material. Briefly, the DMPS is composed of a Differential Mobility Analyzer (DMA) and a Condensation Particle Counter (CPC). The DMA selects narrow particle mobility size ranges from dried (RH≈25 %) polydisperse ambient particles (sampled through PM10 inlet line) and the CPC measures their number concentrations. Particle number concentrations are recorded for 30 logarithmically spaced mobility diameters (from about 20 to 650 nm) during a 32 minute scan (60 s in each mobility diameter and 120 s between scans). The actual ambient particle number size distribution is then inverted from the CPC observations by the user defined routines (Wiedensohler et al., 2012). The inversion routines account mainly for the effects of the DMA transfer function and particle charging efficiencies including multiply charged particles.

The SP2 (see e.g., Stephens et al., 2003; Schwarz et al., 2006; Moteki and Kondo, 2007) was connected in parallel to the CPC to the outlet of the DMA. The SP2 measures number concentrations of particles with and without rBC for each mobility diameter. Any particle can be identified from the scattered laser light while only the rBC-containing particles emit visible light (incandescence). It is expected that the incandescence is originating from rBC, because clear evidence of other refractory species such as as mineral dust was not observed (e.g. varying ratios between wide and narrow band incandescence signals). Scattering and incandescence signal peak heights are proportional to the particle scattering cross section and rBC mass, respectively. The measured single particle rBC masses (0.3–380 fg quantification range) were converted to rBC volume equivalent diameters (briefly just rBC core diameter) by using 1800 $\mathrm{kg\,m^{-3}}$ density (70–740 nm diameter range). These diameters are used even when it is well known that the ambient rBC is not necessarily spherical or compact (e.g., Bond and Bergstrom, 2006; Peng et al., 2016). Number and volume mean rBC core diameters, average rBC mass concentration, and average number concentration of particles with and without rBC were calculated from the single particle data for each mobility diameter. In addition, the number fraction of particles containing rBC was calculated from the number concentrations

of particles with and without rBC. Number (with and without rBC) and rBC mass size distributions were calculated from the corresponding mobility bin average number and mass concentrations using an applied inversion method. The DMPS inversion method is not directly suitable for SP2 data, because noise from mobility size bins close to the SP2 detection limit would have propagated to the relevant size bins. Therefore, we used the DMPS inversion results (number size distributions calculated from the CPC concentrations) to calculate size-dependent scaling factors that convert SP2 concentrations to corresponding size distributions (see the Supplementary Material). Briefly, the size and scan dependent scaling factor is the inverted size distribution divided by the original CPC concentrations, but we have calculated the mode of the scaling factor for each mobility size bin to reduce the variability and to make the SP2 results less dependent on the availability of the CPC data. This correction accounts for the effects of the DMA transfer function and particle charging efficiencies including multiply charged particles based on a typical particle size distribution. Multiply charged particles have also a small effect on the number and volume mean rBC core diameters, but these have been ignored based on visual examination of the rBC core size distributions (see Sect. 3.2).

Current measurement setup has some similarities with those used by Zhang et al. (2016), Liu et al. (2013) and McMeeking et al. (2011), who coupled a SP2 with a Volatility Tandem Differential Mobility Analyzer (VTDMA) and Hygroscopicity Tandem Differential Mobility Analyzer (HTDMA). The VTDMA measures particle size distributions after exposing size-selected (200, 250, 300 and 350 nm) particles to 300 °C temperature (Zhang et al., 2016). The same size-selected particles are also measured by the SP2 allowing comparison between rBC core size distributions and those measured by the VTDMA. In the HTDMA-SP2 setup used by McMeeking et al. (2011) and Liu et al. (2013), size-selected particles (147, 193 and 286 nm in the first study and 163 and 259 nm in the second study) are exposed to a high RH (∼90 %) and then measured by the SP2. There are also studies where the SP2 has been placed behind different types of classifiers such as the Aerosol Particle Mass (APM) analyzer or the Centrifugal Particle Mass Analyzer (CPMA) (e.g., Ohata et al., 2016). The main advantages of the current DMPS-SP2 setup is that the mobility size resolution is better (30 logarithmic size bins from about 20 nm to 650 nm) and this allows the calculation of rBC mass and number size distributions.

Consistency tests showed that the SP2 over counted particles compared with the parallel CPC measurements, which is a known issue for this specific SP2 (Supplementary Material). Multiplying all SP2 concentrations by a factor of 0.82 made the SP2 and CPC number concentrations levels similar with just noise-like variability. Consistency tests also showed that the DMA-selected mobility sizes are in good agreement with those measured by the SP2 (particles without rBC) although a weak dependency on the SP2 temperature was observed (known issue for all SP2s). Comparison between rBC mass concentration with the optically detected (Aethalometer) equivalent BC (eBC) mass concentration from Mukteshwar showed a strong correlation between mass concentrations (absolute values are not directly comparable) and that their ratio was independent of the SP2 temperature. Finally, laser power analysis showed that the average scattering signal was 93 % and 41 % from the original calibration value at Mukteshwar and Gual Pahari, respectively. Especially the latter drop in scattering signal could indicate critical drop in laser power. However, additional calculations showed that the reduced laser power is high enough for detecting rBC from particles with mobility sizes above 200 nm. These consistency tests show that the instrument setup and the data analysis methods provide accurate size-resolved rBC size distributions and mixing state parameters.

3 Results

Any SP2 can measure rBC core mass distributions (i.e. rBC mass concentration as a function of rBC core volume equivalent diameter) with high time resolution, however, the current size-selected measurements give this information for each DMA-selected mobility diameter. Knowing the particle (mobility) size simplifies the calculations especially for rBC-containing particles, which evaporate when travelling through the laser beam. For those particles, Leading Edge Only (LEO) methods (e.g., Gao et al., 2007; Metcalf et al., 2012; Laborde et al., 2012) can be used to calculate the optical size from the scattered laser light, but the calculations require additional particle position information and the results depend on the assumed particle structure and optical parameters. In the following calculations particle size is represented by the DMA-selected mobility diameter. However, optical and mobility sizes are compared in Sect. 3.6 to obtain additional information about particle morphology.

Size-selected measurements allow the detailed examination of the rBC homogeneity, i.e. the variability of the rBC core size within each mobility size bin (Sect. 3.2). Since this level of detail is not typically needed, we will focus on the particle properties averaged for each DMA-selected mobility size bin. These values are used to calculate rBC number and mass size distributions and size-dependent rBC mixing state parameters (number fraction of particles containing rBC and the average rBC core size in those particles) for each size scan. Their average values are described in Sects 3.3 and 3.4 and diurnal cycles in Sect. 3.5. First, we give an overview of the measured parameters and their time variations using the total rBC mass concentration as an example (Sect. 3.1).

3.1 Total rBC mass concentration time series

As an example of the measured parameters and their time variations, the total rBC mass concentration time series from the site at the polluted Indo-Gangetic plains (Gual Pahari) and the relatively clean site at the Himalayan foothills (Mukteshwar) are shown in Fig. 2. Time series of the other parameters, which will be described below, are shown in the Supplementary Material. The average rBC mass concentrations and their standard deviations are 11 ± 11 and 1.0 ± 0.6 $\mu g\,m^{-3}$ for Gual Pahari and Mukteshwar, respectively. Figure 2 shows that the rBC mass concentrations are highly variable, which is the reason for the high standard deviations (absolute measurement uncertainties are close to 20 % (e.g., Laborde et al., 2012)), and the variability is dominated by their diurnal cycles. Statistically significant long term trends or weekly cycles cannot be found. Detailed examination of the diurnal variations of the total rBC mass and the other measured rBC mixing state parameters will be given in Sect. 3.5.

3.2 Size-selected rBC homogeneity

Examining size-selected rBC core size distributions can show how homogeneous these rBC-containing particles are. The selected mobility size must be large enough so that the thickly coated rBC can be detected, but still small enough to represent the accumulation mode particles. Examination of the available mobility sizes showed that the 360 nm mobility diameter is optimal for this purpose (the limits are shown in the Supplementary Material). Figure 3 shows the campaign average rBC core number size distributions from particles with 360 nm DMA-selected mobility diameter (variability shown in the Supplementary

Material). When Gual Pahari rBC core size distribution is mostly unimodal (mode at about 180 nm), that at Mukteshwar is clearly bimodal where the smaller mode is located at about 110 nm and the other dominating mode is at about 210 nm. Changing the DMA-selected diameter to a larger or smaller value does not reveal any additional modes and the same larger mode is always dominating. The modes are relatively wide mainly due to the width of DMA transfer function (the full width at half maximum is about 45 nm for the 360 nm mobility size). The tails of the size distributions are related to the instrument noise (below 85 nm and above 300 nm) and multiply charged particles (above 300 nm), but they have small contributions to the mobility size bin mean values that are used in the following sections (86 % and 92 % of the particles between 85 and 300 nm in Gual Pahari and Mukteshwar, respectively). In general, the modes at about 200 nm seem to be quite similar for Gual Pahari and Mukteshwar while the smaller mode at about 110 nm is clearly seen only at Mukteshwar.

Figure 3 shows the campaign average core size distributions for the 360 nm mobility diameter, but we have also calculated those for each size scan. Mukteshwar rBC core number size distribution seems to be bimodal most of the time. The number fraction of the larger rBC particles (those larger than 140 nm from the 85–300 nm core size range) varies between 0.5 and 0.8. The fluctuations are irregular covering several days, and mainly for this reason, there are no significant diurnal variations (not shown). Since rBC homogeneity within a DMA-selected mobility size bin is too detailed information for most practical applications, following calculations are based on rBC properties averaged for each mobility size bin in each scan.

3.3 Average rBC size distributions

Figure 4 shows the campaign average rBC core mass and number size distributions from the both measurement sites. The gab at about 300 nm is caused by discontinuous high and low gain rBC mass calibration parameterizations. Due to the significant diurnal variations, which will be discussed later, the average mass and number size distributions have standard deviations (not shown) that are proportional to the observed size bin mean values. It is evident from Fig. 4 that the number size distributions are not fully resolved due to the about 70 nm rBC core size detection limit. Therefore, we will focus on the rBC mass size distributions. These have similar shapes except that the concentrations at Gual Pahari are about ten times higher than those at Mukteshwar. Both mass distributions peak at around 210 nm, but these have relatively high concentrations of larger particles especially at Gual Pahari. Large particles are also observed in the number and mass size distributions measured by the DMPS (shown in the Supplementary Material). Bimodal log-normal distributions fitted to the mass distributions are shown with three (both modes and the total) thin blue (Mukteshwar) and green (Gual Pahari) lines in Fig. 4. The fits show that the peak diameters of the main modes are 195 and 202 nm and the main modes cover 76 % and 93 % of the observed rBC mass in Gual Pahari and Mukteshwar, respectively. Because only the tails of the modes with larger particles are seen (their peak diameters are larger than the rBC core detection limit, 740 nm), it is not possible to quantify their contributions to the total rBC mass.

Figure 4 shows the campaign average distributions, but we have also calculated those for each mobility scan. Although the mass distributions are somewhat skewed, these can be described relatively well by log-normal distributions. We have therefore calculated the time series of total rBC mass concentrations (shown in Fig. 2) and geometric mass mean diameters and standard deviations (shown in the Supplementary Material). The average size distribution parameters and their standard deviations

from both measurement sites are shown in Table 1. The diurnal variations of the key rBC size distribution and mixing state parameters are shown in Sect. 3.5.

Previous SP2 studies have reported rBC core size distribution parameters from various environments (e.g. summary in Huang et al., 2012), but to our knowledge there are no previously published results from India. However, equally high rBC concentrations are observed in China and there SP2 studies have shown that rBC core peak diameters are close to 220 nm (Huang et al., 2011, 2012; Wang et al., 2014), which are in good agreement with the current observations (peaks at about 210 nm). Huang et al. (2011) and Wang et al. (2014) have also observed bimodal rBC size distributions, but the larger particles (>400 nm) have significantly higher contribution in India. In general, mass mean diameters are relatively similar at least compared with concentrations which vary by several orders of magnitude depending heavily on local and regional emission sources.

3.4 Average rBC mixing state

Mixing state can be described by two parameters that are directly measured by the SP2: number fraction of particles containing rBC (N_{rBC}/N_{total}) and rBC mass in these particles, which is here represented by the rBC core diameter (volume equivalent diameter based on 1800 $\mathrm{kg\,m^{-3}}$ rBC density). Because core diameters showed some variability (Fig. 3), we have calculated both number and volume mean rBC core diameters ($D_{rBC,N}$ and $D_{rBC,V}$). We also present their ratios with the mobility diameters (D_m). Since these particles may not be spherical (some indirect evidence is given in Sect. 3.6), rBC core to mobility diameter ratios should not be taken as an exact measure of the rBC volume fraction. These parameters depend on mobility size and time, but the time series are correlated. Therefore, conclusions can be made using only one time series and mean values for each mobility size. Again, we use the 360 nm mobility size to represent the typical accumulation mode particles.

The campaign average mixing state parameters and their standard deviations for the 360 nm mobility size are shown in Table 1. As expected, the rBC number fraction is somewhat larger in Gual Pahari (polluted region) than in Mukteshwar (regional background), but the rBC-containing particles seem to have similar rBC core diameters. It could have been expected that rBC core size decreases when secondary aerosol species such as organics and sulfate condense to existing particles during their transport to Mukteshwar, but this effect is not clearly seen, although it may contribute to the observed bimodal rBC core size distribution seen in Fig. 3. It seems that the observed rBC properties are common for the whole region due to the similar emission sources and relatively short times for aging (more likely hours than days). For example, air masses in the upper troposphere or in remote regions can have spent several days without any contact to rBC sources.

There are some previous studies that describe the rBC mixing state with this level of details. It is evident that most particles do not contain detectable amounts of rBC anywhere (e.g., Kondo et al., 2011; Reddington et al., 2013; Dahlkötter et al., 2014; Raatikainen et al., 2015), but the current number fractions of rBC-containing particles (46 % and 31 % for the 360 nm mobility size at Gual Pahari and Mukteshwar, respectively) seem to be the highest so far. For example, our previous results from the Finnish Arctic show that 24 % of the particles from 350–450 nm optical diameter range contain rBC and this is already a relatively large fraction (Raatikainen et al., 2015). In India, the high number fraction of rBC-containing particles is resulting from the significant regional black carbon emissions. The observed rBC core to particle diameter ratios ($D_{rBC,V}/D_m \sim 0.6$

and $D_{rBC,N}/D_m \sim 0.5$ from Table 1), which cube is rBC volume fraction in a spherical compact particle, are larger than those observed for aged aerosol (e.g., Raatikainen et al., 2015; Dahlkötter et al., 2014), but match with the lowest values found for fresh emissions (e.g., Kondo et al., 2011; Schwarz et al., 2008; Sahu et al., 2012; Metcalf et al., 2012). For example, Metcalf et al. (2012) found thickly coated rBC from an urban plume with rBC core to particle diameter ratios ranging from about 0.51 to 0.59 (145 nm rBC cores with 50–70 nm coating thicknesses). Although the agreement is good, it should be noted that our particle size is based on the mobility diameter while most other studies use the optical diameter from the LEO method. We will show later (Sect. 3.6) that mobility sizes are larger than optical sizes, which means that our rBC core to particle (optical) diameter ratios actually represent fresh emissions.

Mixing state parameters are somewhat size-dependent and this can be parameterized using the size-selected measurements. Fig. 5 shows the averaged size dependent mixing state parameters (number and volume based rBC core diameters and number fractions of particles containing rBC) and simple parameterizations. The lowest particle sizes where the SP2 detection limit has a significant effect on the results have been excluded from the fits (indicated by the smaller marker below ∼200 nm particle size). Also, the largest particle size in Mukteshwar has also been excluded due to the low number of observed particles. In general, the trends in the rBC mixing state parameters are similar for Gual Pahari and Mukteshwar, which indicates fairly similar local and regional rBC sources.

3.5 Diurnal cycles

Figure 6 shows the diurnal cycles of the rBC mass distribution (total mass and geometric mass mean diameter and standard deviation) and mixing state (rBC core to mobility diameter ratio and the number fraction of particles containing rBC for the 360 nm mobility size) parameters. The number based diameter ratios and size distribution parameters are not shown, because these have similar diurnal variations with the mass and volume based parameters. The total rBC mass concentrations have significant diurnal variations while those for the mean diameter and distribution width are modest. From the rBC mixing state parameters, which are not directly related to the mass distribution, only the rBC particle number fractions have clear diurnal cycles while the rBC core to mobility diameter ratio is practically constant. The strong diurnal variability of the rBC mass concentrations is in good agreement with those of equivalent black carbon observed in our previous studies and by others (e.g., Komppula et al., 2009; Hyvärinen et al., 2009, 2010; Panwar et al., 2013; Raatikainen et al., 2014). Increased vertical mixing is the main reason for the daytime decrease in rBC mass in Gual Pahari and this can also explain the decrease in rBC number fraction. In general, Gual Pahari and Mukteshwar rBC aerosols are relatively similar except that the Gual Pahari aerosol has an order of magnitude higher concentration and the number fraction of particles containing rBC is about 50 % larger compared with those from Mukteshwar.

3.6 Morphology of rBC-containing particles

Black carbon or soot particles are initially aggregates composed of several primary BC particles, which diameters are in the order of a few tens of nanometers (e.g., Sorensen, 2001). These fresh aggregates can contain some amounts of a non-refractory material, but the fraction increases with time when atmospheric vapours condense to the soot particles and when the particle

grows by coagulation. Increasing non-refractory fraction makes these particles more spherical. In addition, aggregates can be compacted when particles absorb water vapour and become droplets (e.g., Zhang et al., 2008; Pagels et al., 2009). As a result, core-shell structure can be a valid approximation for the aged aerosol, but it is not clear if this is the case in India, where the aerosol is relatively fresh. The SP2 can provide some information about the morphology of the rBC-containing particles.

First, the SP2 can detect if a particle disintegrates in the laser beam into rBC and non-rBC fragments. This can happen if the rBC core is close to the particle surface or when rBC is attached to the surface of another particle (Sedlacek et al., 2012; Moteki et al., 2014). However, our measurements show that such disintegrating particles have negligible concentrations.

There are also studies reporting bare rBC particles (e.g., Huang et al., 2012), but the current rBC core volume equivalent diameters are always well below mobility diameters. However, it is possible that the rBC particles have low densities or that the particles are irregular aggregates. At least qualitative information about the particle shape can be obtained by comparing the DMA-selected mobility and SP2-derived optical sizes. Optical size is based on the measured or reconstructed (see below) intensity of the scattered laser light and a theoretical correction to the scattering accounting for the difference between calibration (ammonium sulfate) and ambient aerosol structures and optical properties. Accurate sizing requires information about particle structure, but clear differences (e.g. much larger than the typical $\pm$20 % sizing uncertainty) between optical and mobility sizes indicate non-spherical particles such as aggregates.

3.6.1 Optical size based on a LEO method

Optical sizes are estimated using Leading Edge Only (LEO) methods (e.g., Gao et al., 2007; Metcalf et al., 2012; Laborde et al., 2012). In earlier studies, the authors use the leading edge of the scattering signal, which is yet unaffected by the evaporation of the non-refractory material, to reconstruct the unperturbed scattering signal. Current method is the same as the method used in our previous study (Raatikainen et al., 2015): here the leading edge is the part of the signal where laser beam intensity is 0.07–3 % of the maximum, and the Gaussian scattering (laser beam) profile and peak position are calculated by averaging those from 100 previous particles that do not have detectable incandescence signal. Scattering signal peak height is solved by fitting the Gaussian profile to the signal from the leading edge (e.g., Gao et al., 2007). Scattering cross section is calculated from the signal peak height by using the scattering calibration, and optical particle size is calculated from the scattering cross section by using the Mie theory (linear interpolation between the limits of pure ammonium sulfate (refractive index m=1.48-i0) and a mixed particle (m=1.715-i0.395) with rBC core to particle diameter ratio of 0.6).

The current LEO analysis suffered from a systematic noise signal, which increased the variability of the results and seemed to cause a systematic bias when the instrument temperature was below 30 °C (see the Supplementary Material). Also, the decrease in laser power when the SP2 was transported from Mukteshwar to Gual Pahari decreased the success rate of the LEO fits from 98.6 % to 90.9 % (for rBC-containing particles from the 360 nm mobility size bin). Due to these uncertainties, we focus on the 360 nm mobility size bin and use data from instrument temperatures between 30 and 35 °C. These results seem to be reliable, but potential biases cannot be fully ruled out.

For the 360 nm mobility size and when the instrument temperature is between 30 and 35 °C, the campaign average LEO-derived optical particle diameters for rBC-containing particles are 245$\pm$10 and 234$\pm$20 nm for Mukteshwar and Gual Pahari,

respectively. For reference, corresponding sizes for particles without rBC are 360±25 and 359±17 nm, which are in good agreement with those without the LEO method (356±7 and 361±11 nm) and the selected mobility diameter (360 nm). It is clear that the average optical size is significantly smaller than the mobility size, which shows that the rBC-containing particles are not spherical. Further examination of the single particle data can reveal additional details about individual particles. Figure 7 shows the dependency of the optical size on the rBC core size by means of a probability density map (~~darker color means higher probability~~normalized by the maximum probability density). The rBC core size population is clearly bimodal in Mukteshwar (see Sect. 3.2) and it seems that the smaller rBC cores are thickly coated (core to optical diameter ratio approx. 0.4) while the larger rBC cores are thinly coated (core to optical diameter ratio close to unity). The only clear rBC mode in Gual Pahari seems to be thinly coated. The red markers and error bars show the effect of refractive index on the calculated optical size; the upper limit is based on ammonium sulfate refractive index (m=1.48-i0) and the lower limit is based on that of pure rBC (m=2.26-i1.26 from Moteki et al. (2010)). Additional uncertainties arise from the particle morphology (e.g. He et al., 2015) and scattering model (e.g. He et al., 2016). Even when considering these large potential uncertainties, the optical sizes are smaller than the mobility sizes, which show that rBC-containing particles are not spherical. Especially the thinly coated particles are most likely highly fractal soot aggregates. Such aggregates typically have low volume fractions of non-refractory material, but the exact fractions cannot be determined without detailed information about particle morphology and optical properties (e.g. He et al., 2016).

Zhang et al. (2016) used similar measurement setup (VTDMA-SP2) in northern China about 60 km from Beijing. They have found closely matching LEO-calculated optical and mobility sizes, which indicates spherical particle shape, and internally mixed particles with low rBC volume fraction (161 nm mass equivalent rBC core size for 350 nm mobility size). Although the rBC concentrations have similar magnitudes in northern China and India, rBC-containing particles seem to have different properties most likely due to different sources.

4 Conclusions

Refractory black carbon (rBC) mass distributions and mixing state parameters were measured using a size-selected Single Particle Soot Photometer (SP2) in northern India during spring 2014. The size-selected results were obtained by connecting a SP2 to the outlet of a Differential Mobility Analyzer (DMA), which classifies particles according to their mobility size. The measurements were made in a relatively clean regional background site at the Himalayan foothills (Mukteshwar) and at a relatively polluted site close to Delhi (Gual Pahari). To our knowledge, this is the first publication showing size-selected rBC mass distributions and mixing state parameters for this region.

The measurements show that 46±12 % and 31±5 % of the accumulation mode particles contain observable amounts of rBC in Gual Pahari and Mukteshwar, respectively. Just as the absolute rBC concentrations (11±11 and 1.0±0.6 $\mu g\,m^{-3}$ in Gual Pahari and Mukteshwar, respectively), the rBC particle number fraction is higher at the source region (represented by Gual Pahari) and lower at elevated altitudes (Mukteshwar). Although literature data about rBC mixing state is limited (e.g.,

Raatikainen et al., 2015; Dahlkötter et al., 2014; Reddington et al., 2013), the observed number fractions of particles containing rBC are the highest reported so far.

The observed rBC particles are likely to contain non-refractory materials such as sulfate and organics, but the exact volume fractions could not be quantified, because these particles are not spherical. Current rBC volume equivalent to mobility diameter ratios (number mean $D_{rBC,N}/D_m$ are 0.51±0.02 and 0.50±0.03 for Gual Pahari and Mukteshwar, respectively) would mean that spherical particles have lower rBC volume fractions than expected for fresh particles (e.g., Schwarz et al., 2008; Sahu et al., 2012). However, optical sizes determined using a Leading Edge Only (LEO) method were significantly smaller than the mobility diameters, which indicates that the rBC-containing particles are highly irregular such as fractal aggregates. The rBC diameter to optical size ratios (∼0.8 at Gual Pahari and ∼0.7 at Mukteshwar) are closer to value expected for fresh aerosol, but these calculations are also limited by the fact that the optical size is based on assumed optical parameters and spherical core-shell structure. The exact calculation of particle composition is not possible without additional details about particle structure.

Although individual particles seem to be quite similar in Gual Pahari and Mukteshwar, the total rBC concentrations are about ten times higher at the more polluted site, Gual Pahari, than those at the regional background site, Mukteshwar. Also, a larger fraction of the particles contain rBC in Gual Pahari than in Mukteshwar. One explanation for the similarity is that some aerosol sources are common for the whole region (e.g. crop residue and biofuel burning and cooking). The other is that a significant fraction of the rBC seen in Mukteshwar can be originating from the densely populated Indo-Gangetic plains represented by Gual Pahari (Raatikainen et al., 2014).

Detailed information about the black carbon mixing state is needed for assessing and improving the performance of climate models in simulating their evolution and radiative effects. SP2 is one of the few instruments that can provide detailed information about the rBC mixing state. The accuracy of the mixing state parameters can be further improved by size-selecting the particles before measurements with the SP2; this method is especially suitable for polluted areas where good counting statistics is guaranteed.

Acknowledgements. Authors would like to acknowledge the Academy of Finland (project numbers 264242, 268004 and 284536), Academy of Finland Centre of Excellence Program (project number 272041) and KONE foundation for the financial support. We thank to local TERI staff for 24/7 work at Mukteshwar aerosol research station.

References

Adachi, K., Chung, S. H., and Buseck, P. R.: Shapes of soot aerosol particles and implications for their effects on climate, J. Geophys. Res., 115, D15 206, doi:10.1029/2009JD012868, 2010.

Bollasina, M., Nigam, S., and Lau, K.-M.: Absorbing Aerosols and Summer Monsoon Evolution over South Asia: An Observational Portrayal, J. Clim., 21, 3221–3239, doi:10.1175/2007JCLI2094.1, 2008.

Bollasina, M. A., Ming, Y., and Ramaswamy, V.: Anthropogenic Aerosols and the Weakening of the South Asian Summer Monsoon, Science, 334, 502–505, doi:10.1126/science.1204994, 2011.

Bond, T. C. and Bergstrom, R. W.: Light Absorption by Carbonaceous Particles: An Investigative Review, Aerosol Sci. Tech., 40, 27–67, doi:10.1080/02786820500421521, 2006.

Bond, T. C., Doherty, S. J., Fahey, D. W., Forster, P. M., Berntsen, T., DeAngelo, B. J., Flanner, M. G., Ghan, S., Kärcher, B., Koch, D., Kinne, S., Kondo, Y., Quinn, P. K., Sarofim, M. C., Schultz, M. G., Schulz, M., Venkataraman, C., Zhang, H., Zhang, S., Bellouin, N., Guttikunda, S. K., Hopke, P. K., Jacobson, M. Z., Kaiser, J. W., Klimont, Z., Lohmann, U., Schwarz, J. P., Shindell, D., Storelvmo, T., Warren, S. G., and Zender, C. S.: Bounding the role of black carbon in the climate system: A scientific assessment, J. Geophys. Res.-Atmos., 118, 5380–5552, doi:10.1002/jgrd.50171, 2013.

Boos, W. R. and Storelvmo, T.: Near-linear response of mean monsoon strength to a broad range of radiative forcings, P. Natl. Acad. Sci. USA, 113, 1510–1515, doi:10.1073/pnas.1517143113, 2016.

Cappa, C. D., Onasch, T. B., Massoli, P., Worsnop, D. R., Bates, T. S., Cross, E. S., Davidovits, P., Hakala, J., Hayden, K. L., Jobson, B. T., Kolesar, K. R., Lack, D. A., Lerner, B. M., Li, S.-M., Mellon, D., Nuaaman, I., Olfert, J. S., Petäjä, T., Quinn, P. K., Song, C., Subramanian, R., Williams, E. J., and Zaveri, R. A.: Radiative Absorption Enhancements Due to the Mixing State of Atmospheric Black Carbon, Science, 337, 1078–1081, doi:10.1126/science.1223447, 2012.

Cross, E. S., Onasch, T. B., Ahern, A., Wrobel, W., Slowik, J. G., Olfert, J., Lack, D. A., Massoli, P., Cappa, C. D., Schwarz, J. P., Spackman, J. R., Fahey, D. W., Sedlacek, A., Trimborn, A., Jayne, J. T., Freedman, A., Williams, L. R., Ng, N. L., Mazzoleni, C., Dubey, M., Brem, B., Kok, G., Subramanian, R., Freitag, S., Clarke, A., Thornhill, D., Marr, L. C., Kolb, C. E., Worsnop, D. R., and Davidovits, P.: Soot Particle Studies–Instrument Inter-Comparison–Project Overview, Aerosol Sci. Tech., 44, 592–611, doi:10.1080/02786826.2010.482113, 2010.

Dahlkötter, F., Gysel, M., Sauer, D., Minikin, A., Baumann, R., Seifert, P., Ansmann, A., Fromm, M., Voigt, C., and Weinzierl, B.: The Pagami Creek smoke plume after long-range transport to the upper troposphere over Europe – aerosol properties and black carbon mixing state, Atmos. Chem. Phys., 14, 6111–6137, doi:10.5194/acp-14-6111-2014, 2014.

D'Errico, M., Cagnazzo, C., Fogli, P. G., Lau, W. K. M., von Hardenberg, J., Fierli, F., and Cherchi, A.: Indian monsoon and the elevated-heat-pump mechanism in a coupled aerosol-climate model, J. Geophys. Res.-Atmos., 120, 8712–8723, doi:10.1002/2015JD023346, 2015.

Ganguly, D., Rasch, P. J., Wang, H., and Yoon, J.-H.: Climate response of the South Asian monsoon system to anthropogenic aerosols, J. Geophys. Res.-Atmos., 117, D13 209, doi:10.1029/2012JD017508, 2012.

Gao, R. S., Schwarz, J. P., Kelly, K. K., Fahey, D. W., Watts, L. A., Thompson, T. L., Spackman, J. R., Slowik, J. G., Cross, E. S., Han, J.-H., Davidovits, P., Onasch, T. B., and Worsnop, D. R.: A Novel Method for Estimating Light-Scattering Properties of Soot Aerosols Using a Modified Single-Particle Soot Photometer, Aerosol Sci. Tech., 41, 125–135, doi:10.1080/02786820601118398, 2007.

Gautam, R., Hsu, N. C., Lau, K.-M., and Kafatos, M.: Aerosol and rainfall variability over the Indian monsoon region: distributions, trends and coupling, Ann. Geophys., 27, 3691–3703, doi:10.5194/angeo-27-3691-2009, 2009.

He, C., Liou, K.-N., Takano, Y., Zhang, R., Levy Zamora, M., Yang, P., Li, Q., and Leung, L. R.: Variation of the radiative properties during black carbon aging: theoretical and experimental intercomparison, Atmos. Chem. Phys., 15, 11 967–11 980, doi:10.5194/acp-15-11967-2015, 2015.

He, C., Takano, Y., Liou, K.-N., Yang, P., Li, Q., and Mackowski, D. W.: Intercomparison of the GOS approach, superposition T-matrix method, and laboratory measurements for black carbon optical properties during aging, J. Quant. Spectrosc. Ra., 184, 287–296, doi:10.1016/j.jqsrt.2016.08.004, 2016.

Hooda, R., Hyvärinen, A.-P., Vestenius, M., Gilardoni, S., Sharma, V., Vignati, E., Kulmala, M., and Lihavainen, H.: Atmospheric aerosols local–regional discrimination for a semi-urban area in India, Atmos. Res., 168, 13–23, doi:10.1016/j.atmosres.2015.08.014, 2016.

Huang, X.-F., Gao, R. S., Schwarz, J. P., He, L.-Y., Fahey, D. W., Watts, L. A., McComiskey, A., Cooper, O. R., Sun, T.-L., Zeng, L.-W., Hu, M., and Zhang, Y.-H.: Black carbon measurements in the Pearl River Delta region of China, J. Geophys. Res.-Atmos., 116, doi:10.1029/2010JD014933, 2011.

Huang, X.-F., Sun, T.-L., Zeng, L.-W., Yu, G.-H., and Luan, S.-J.: Black carbon aerosol characterization in a coastal city in South China using a single particle soot photometer, Atmos. Environ., 51, 21–28, doi:10.1016/j.atmosenv.2012.01.056, 2012.

Hyvärinen, A.-P., Lihavainen, H., Komppula, M., Sharma, V. P., Kerminen, V.-M., Panwar, T. S., and Viisanen, Y.: Continuous measurements of optical properties of atmospheric aerosols in Mukteshwar, northern India, J. Geophys. Res., 114, D08 207, doi:10.1029/2008JD011489, 2009.

Hyvärinen, A.-P., Lihavainen, H., Komppula, M., Panwar, T. S., Sharma, V. P., Hooda, R. K., and Viisanen, Y.: Aerosol measurements at the Gual Pahari EUCAARI station: preliminary results from in-situ measurements, Atmos. Chem. Phys., 10, 7241–7252, doi:10.5194/acp-10-7241-2010, 2010.

Komppula, M., Lihavainen, H., Hyvärinen, A.-P., Kerminen, V.-M., Panwar, T. S., Sharma, V. P., and Viisanen, Y.: Physical properties of aerosol particles at a Himalayan background site in India, J. Geophys. Res., 114, D12 202, doi:10.1029/2008JD011007, 2009.

Kondo, Y., Matsui, H., Moteki, N., Sahu, L., Takegawa, N., Kajino, M., Zhao, Y., Cubison, M. J., Jimenez, J. L., Vay, S., Diskin, G. S., Anderson, B., Wisthaler, A., Mikoviny, T., Fuelberg, H. E., Blake, D. R., Huey, G., Weinheimer, A. J., Knapp, D. J., and Brune, W. H.: Emissions of black carbon, organic, and inorganic aerosols from biomass burning in North America and Asia in 2008, J. Geophys. Res.-Atmos., 116, D08 204, doi:10.1029/2010JD015152, 2011.

Laborde, M., Mertes, P., Zieger, P., Dommen, J., Baltensperger, U., and Gysel, M.: Sensitivity of the Single Particle Soot Photometer to different black carbon types, Atmos. Meas. Tech., 5, 1031–1043, doi:10.5194/amt-5-1031-2012, 2012.

Lack, D., Moosmüller, H., McMeeking, G., Chakrabarty, R., and Baumgardner, D.: Characterizing elemental, equivalent black, and refractory black carbon aerosol particles: a review of techniques, their limitations and uncertainties, Anal. Bioanal. Chem., 406, 99–122, doi:10.1007/s00216-013-7402-3, 2014.

Lau, W. K. M., Kim, M.-K., Kim, K.-M., and Lee, W.-S.: Enhanced surface warming and accelerated snow melt in the Himalayas and Tibetan Plateau induced by absorbing aerosols, Environ. Res. Lett., 5, 025 204, 2010.

Liu, D., Allan, J., Whitehead, J., Young, D., Flynn, M., Coe, H., McFiggans, G., Fleming, Z. L., and Bandy, B.: Ambient black carbon particle hygroscopic properties controlled by mixing state and composition, Atmos. Chem. Phys., 13, 2015–2029, doi:10.5194/acp-13-2015-2013, 2013.

McMeeking, G. R., Good, N., Petters, M. D., McFiggans, G., and Coe, H.: Influences on the fraction of hydrophobic and hydrophilic black carbon in the atmosphere, Atmos. Chem. Phys., 11, 5099–5112, doi:10.5194/acp-11-5099-2011, 2011.

Menon, S., Hansen, J., Nazarenko, L., and Luo, Y.: Climate Effects of Black Carbon Aerosols in China and India, Science, 297, 2250–2253, doi:10.1126/science.1075159, 2002.

Metcalf, A. R., Craven, J. S., Ensberg, J. J., Brioude, J., Angevine, W., Sorooshian, A., Duong, H. T., Jonsson, H. H., Flagan, R. C., and Seinfeld, J. H.: Black carbon aerosol over the Los Angeles Basin during CalNex, J. Geophys. Res.-Atmos., 117, D00V13, doi:10.1029/2011JD017255, 2012.

Moteki, N. and Kondo, Y.: Effects of Mixing State on Black Carbon Measurements by Laser-Induced Incandescence, Aerosol Sci. Tech., 41, 398–417, doi:10.1080/02786820701199728, 2007.

Moteki, N., Kondo, Y., and Nakamura, S.: Method to measure refractive indices of small nonspherical particles: Application to black carbon particles, J. Aerosol Sci., 41, 513–521, doi:10.1016/j.jaerosci.2010.02.013, 2010.

Moteki, N., Kondo, Y., and Adachi, K.: Identification by single-particle soot photometer of black carbon particles attached to other particles: Laboratory experiments and ground observations in Tokyo, J. Geophys. Res.-Atmos., 119, 1031–1043, doi:10.1002/2013JD020655, 2014.

Ohata, S., Schwarz, J. P., Moteki, N., Koike, M., Takami, A., and Kondo, Y.: Hygroscopicity of materials internally mixed with black carbon measured in Tokyo, J. Geophys. Res.-Atmos., 121, 362–381, doi:10.1002/2015JD024153, 2016.

Pagels, J., Khalizov, A. F., McMurry, P. H., and Zhang, R. Y.: Processing of Soot by Controlled Sulphuric Acid and Water Condensation–Mass and Mobility Relationship, Aerosol Sci. Tech., 43, 629–640, doi:10.1080/02786820902810685, 2009.

Panwar, T., Hooda, R. K., Lihavainen, H., Hyvärinen, A., Sharma, V., and Viisanen, Y.: Atmospheric aerosols at a regional background Himalayan site–Mukteshwar, India, Environmental Monitoring and Assessment, 185, 4753–4764, doi:10.1007/s10661-012-2902-8, 2013.

Peng, J., Hu, M., Guo, S., Du, Z., Zheng, J., Shang, D., Levy Zamora, M., Zeng, L., Shao, M., Wu, Y.-S., Zheng, J., Wang, Y., Glen, C. R., Collins, D. R., Molina, M. J., and Zhang, R.: Markedly enhanced absorption and direct radiative forcing of black carbon under polluted urban environments, P. Natl. Acad. Sci. USA, 113, 4266–4271, doi:10.1073/pnas.1602310113, 2016.

Petzold, A., Ogren, J. A., Fiebig, M., Laj, P., Li, S.-M., Baltensperger, U., Holzer-Popp, T., Kinne, S., Pappalardo, G., Sugimoto, N., Wehrli, C., Wiedensohler, A., and Zhang, X.-Y.: Recommendations for reporting "black carbon" measurements, Atmos. Chem. Phys., 13, 8365–8379, doi:10.5194/acp-13-8365-2013, 2013.

Raatikainen, T., Hyvärinen, A.-P., Hatakka, J., Panwar, T., Hooda, R., Sharma, V., and Lihavainen, H.: The effect of boundary layer dynamics on aerosol properties at the Indo-Gangetic plains and at the foothills of the Himalayas, Atmos. Environ., 89, 548–555, doi:10.1016/j.atmosenv.2014.02.058, 2014.

Raatikainen, T., Brus, D., Hyvärinen, A.-P., Svensson, J., Asmi, E., and Lihavainen, H.: Black carbon concentrations and mixing state in the Finnish Arctic, Atmos. Chem. Phys., 15, 10 057–10 070, doi:10.5194/acp-15-10057-2015, 2015.

Ramanathan, V., Crutzen, P. J., Lelieveld, J., Mitra, A. P., Althausen, D., Anderson, J., Andreae, M. O., Cantrell, W., Cass, G. R., Chung, C. E., Clarke, A. D., Coakley, J. A., Collins, W. D., Conant, W. C., Dulac, F., Heintzenberg, J., Heymsfield, A. J., Holben, B., Howell, S., Hudson, J., Jayaraman, A., Kiehl, J. T., Krishnamurti, T. N., Lubin, D., McFarquhar, G., Novakov, T., andI. A. Podgorny, J. A. O., Prather, K., Priestley, K., Prospero, J. M., Quinn, P. K., Rajeev, K., Rasch, P., Rupert, S., Sadourny, R., Satheesh, S. K., Shaw, G. E., Sheridan, P., and Valero, F. P. J.: Indian Ocean Experiment: An integrated analysis of the climate forcing and effects of the great Indo-Asian haze, J. Geophys. Res., 106, 28 371–28 398, 2001.

Ramanathan, V., Li, F., Ramana, M. V., Praveen, P. S., Kim, D., Corrigan, C. E., Nguyen, H., Stone, E. A., Schauer, J. J., Carmichael, G. R., Adhikary, B., and Yoon, S. C.: Atmospheric brown clouds: Hemispherical and regional variations in long-range transport, absorption, and radiative forcing, J. Geophys. Res., 112, D22S21, doi:10.1029/2006JD008124, 2007.

Reddington, C. L., McMeeking, G., Mann, G. W., Coe, H., Frontoso, M. G., Liu, D., Flynn, M., Spracklen, D. V., and Carslaw, K. S.: The mass and number size distributions of black carbon aerosol over Europe, Atmos. Chem. Phys., 13, 4917–4939, doi:10.5194/acp-13-4917-2013, 2013.

Sahu, L. K., Kondo, Y., Moteki, N., Takegawa, N., Zhao, Y., Cubison, M. J., Jimenez, J. L., Vay, S., Diskin, G. S., Wisthaler, A., Mikoviny, T., Huey, L. G., Weinheimer, A. J., and Knapp, D. J.: Emission characteristics of black carbon in anthropogenic and biomass burning plumes over California during ARCTAS-CARB 2008, J. Geophys. Res.-Atmos., 117, doi:10.1029/2011JD017401, 2012.

Schwarz, J. P., Gao, R. S., Fahey, D. W., Thomson, D. S., Watts, L. A., Wilson, J. C., Reeves, J. M., Darbeheshti, M., Baumgardner, D. G., Kok, G. L., Chung, S. H., Schulz, M., Hendricks, J., Lauer, A., Kärcher, B., Slowik, J. G., Rosenlof, K. H., Thompson, T. L., Langford, A. O., Loewenstein, M., and Aikin, K. C.: Single-particle measurements of midlatitude black carbon and light-scattering aerosols from the boundary layer to the lower stratosphere, J. Geophys. Res.-Atmos., 111, D16 207, doi:10.1029/2006JD007076, 2006.

Schwarz, J. P., Gao, R. S., Spackman, J. R., Watts, L. A., Thomson, D. S., Fahey, D. W., Ryerson, T. B., Peischl, J., Holloway, J. S., Trainer, M., Frost, G. J., Baynard, T., Lack, D. A., de Gouw, J. A., Warneke, C., and Del Negro, L. A.: Measurement of the mixing state, mass, and optical size of individual black carbon particles in urban and biomass burning emissions, Geophys. Res. Lett., 35, L13 810, doi:10.1029/2008GL033968, 2008.

Sedlacek, A. J., Lewis, E. R., Kleinman, L., Xu, J., and Zhang, Q.: Determination of and evidence for non-core-shell structure of particles containing black carbon using the Single-Particle Soot Photometer (SP2), Geophys. Res. Lett., 39, L06 802, doi:10.1029/2012GL050905, 2012.

Slowik, J. G., Cross, E. S., Han, J.-H., Davidovits, P., Onasch, T. B., Jayne, J. T., Williams, L. R., Canagaratna, M. R., Worsnop, D. R., Chakrabarty, R. K., Moosmüller, H., Arnott, W. P., Schwarz, J. P., Gao, R.-S., Fahey, D. W., Kok, G. L., and Petzold, A.: An Inter-Comparison of Instruments Measuring Black Carbon Content of Soot Particles, Aerosol Sci. Tech., 41, 295–314, doi:10.1080/02786820701197078, 2007.

Sorensen, C. M.: Light Scattering by Fractal Aggregates: A Review, Aerosol Sci. Tech., 35, 648–687, doi:10.1080/02786820117868, 2001.

Stephens, M., Turner, N., and Sandberg, J.: Particle identification by laser-induced incandescence in a solid-state laser cavity, Appl. Opt., 42, 3726–3736, doi:10.1364/AO.42.003726, 2003.

Stocker, T., Qin, D., Plattner, G.-K., Tignor, M., Allen, S., Boschung, J., Nauels, A., Xia, Y., Bex, V., and Midgley, P., eds.: Climate Change 2013: The Physical Science Basis. Contribution of Working Group I to the Fifth Assessment Report of the Intergovernmental Panel on Climate Change, Cambridge University Press, Cambridge, United Kingdom and New York, NY, USA, 1535 pp., 2013.

Taylor, J. W., Allan, J. D., Liu, D., Flynn, M., Weber, R., Zhang, X., Lefer, B. L., Grossberg, N., Flynn, J., and Coe, H.: Assessment of the sensitivity of core/shell parameters derived using the single-particle soot photometer to density and refractive index, Atmos. Meas. Tech., 8, 1701–1718, doi:10.5194/amt-8-1701-2015, 2015.

Wang, Q., Schwarz, J.P., Cao, J., Gao, R., Fahey, D.W., Hu, T., Huang, R.-J., Han, Y. and Shen, Z.: Black carbon aerosol characterization in a remote area of Qinghai–Tibetan Plateau, western China, Sci. Total Environ., 1, 151–158, doi:10.1016/j.scitotenv.2014.01.098, 2014.

Wiedensohler, A., Birmili, W., Nowak, A., Sonntag, A., Weinhold, K., Merkel, M., Wehner, B., Tuch, T., Pfeifer, S., Fiebig, M., Fjäraa, A. M., Asmi, E., Sellegri, K., Depuy, R., Venzac, H., Villani, P., Laj, P., Aalto, P., Ogren, J. A., Swietlicki, E., Williams, P., Roldin, P., Quincey, P., Hüglin, C., Fierz-Schmidhauser, R., Gysel, M., Weingartner, E., Riccobono, F., Santos, S., Grüning, C., Faloon, K., Beddows, D., Harrison, R., Monahan, C., Jennings, S. G., O'Dowd, C. D., Marinoni, A., Horn, H.-G., Keck, L., Jiang, J., Scheckman, J., McMurry, P. H., Deng, Z., Zhao, C. S., Moerman, M., Henzing, B., de Leeuw, G., Löschau, G., and Bastian, S.: Mobility particle size spectrometers:

harmonization of technical standards and data structure to facilitate high quality long-term observations of atmospheric particle number size distributions, Atmos. Meas. Tech., 5, 657–685, doi:10.5194/amt-5-657-2012, 2012.

Zhang, R., Khalizov, A. F., Pagels, J., Zhang, D., Xue, H., and McMurry, P. H.: Variability in morphology, hygroscopicity, and optical properties of soot aerosols during atmospheric processing, P. Natl. Acad. Sci. USA, 105, 10 291–10 296, doi:10.1073/pnas.0804860105, 2008.

Zhang, Y., Zhang, Q., Cheng, Y., Su, H., Kecorius, S., Wang, Z., Wu, Z., Hu, M., Zhu, T., Wiedensohler, A., and He, K.: Measuring the morphology and density of internally mixed black carbon with SP2 and VTDMA: new insight into the absorption enhancement of black carbon in the atmosphere, Atmos. Meas. Tech., 9, 1833–1843, doi:10.5194/amt-9-1833-2016, 2016.

Table 1. Campaign average values ($\pm$ standard deviations) describing rBC mass size distributions (total mass and geometric mass mean diameter and standard deviation) and mixing state (number and volume mean core diameters, those normalized by the mobility size (D_m), and number fraction of particles containing rBC). The mixing state parameters are calculated for the 360 nm mobility size bins.

Parameter	Gual Pahari	Mukteshwar
Total rBC ($\mu g\,m^{-3}$)	11 ± 11	1.0 ± 0.6
GMD dm/dlogD_{rBC} (nm)	249 ± 30	217 ± 13
GSD dm/dlogD_{rBC}	0.246 ± 0.014	0.221 ± 0.014
$D_{rBC,N}$ (nm)	185 ± 8	178 ± 12
$D_{rBC,N}/D_m$	0.51 ± 0.02	0.50 ± 0.03
$D_{rBC,V}$ (nm)	221 ± 14	205 ± 16
$D_{rBC,V}/D_m$	0.61 ± 0.04	0.57 ± 0.04
N_{rBC}/N_{total}	0.46 ± 0.12	0.31 ± 0.05

Figure 1. Locations of Gual Pahari (red marker) and Mukteshwar (blue marker) measurement stations.

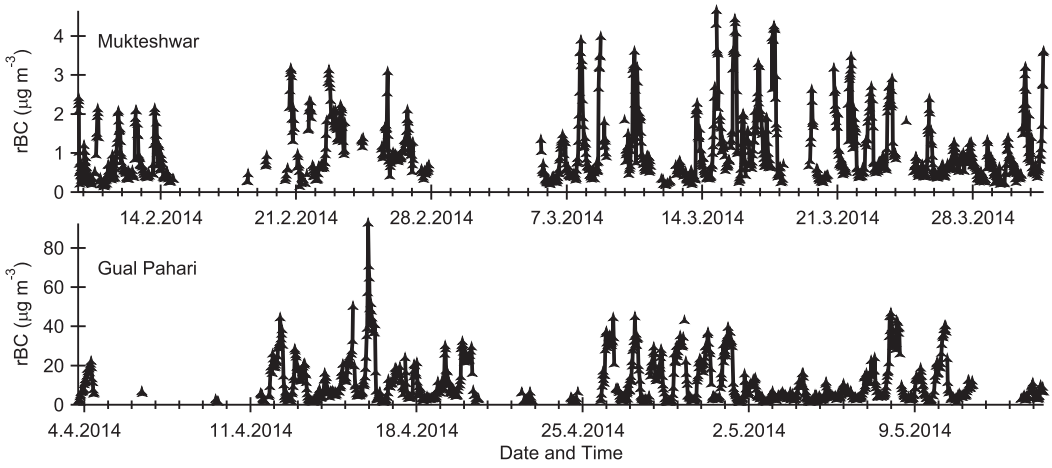

Figure 2. Total rBC mass concentration time series from Mukteshwar (top graph) and Gual Pahari (bottom graph).

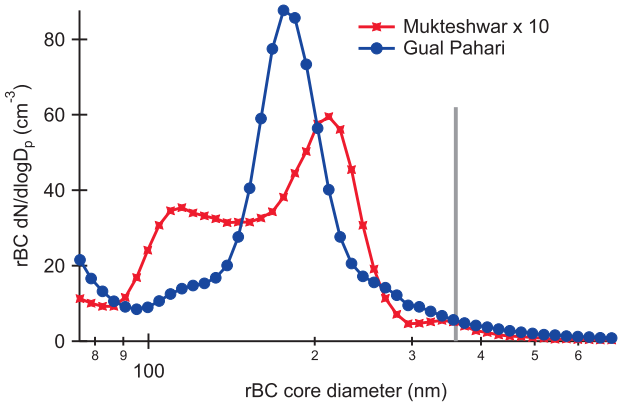

Figure 3. Campaign average rBC core number size distributions for the 360 nm DMA-selected mobility diameter (indicated by the vertical gray line) from Mukteshwar (multiplied by a factor of ten) and Gual Pahari. Standard deviations are approximately equal with the average concentration values when concentrations are larger than 1 cm^{-3} while smaller concentrations mean increasing standard deviations.

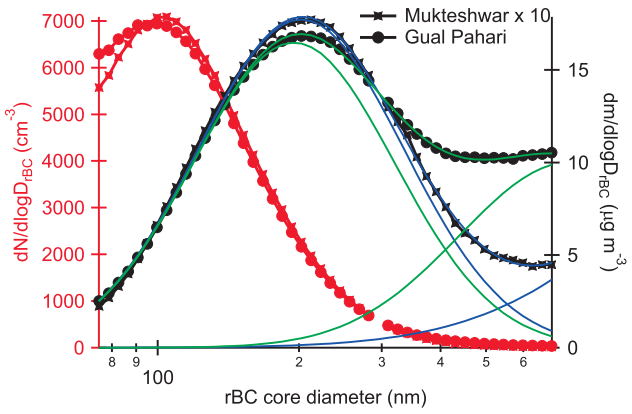

Figure 4. Campaign average rBC mass (black color, right axis) and number (red color, left axis) size distributions for Mukteshwar (lines with circles) and Gual Pahari (lines with crosses). The thin lines are bimodal log-normal fits including both modes and the total fitted mass (blue line for Mukteshwar and green line for Gual Pahari). Mukteshwar number and mass size distributions have been multiplied by a factor of ten. Standard deviations are approximately 80 % (Mukteshwar) or 100 % (Gual Pahari) of the bin mean number and mass. The gab at about 300 nm is caused by discontinuous high and low gain rBC mass calibration parameterizations.

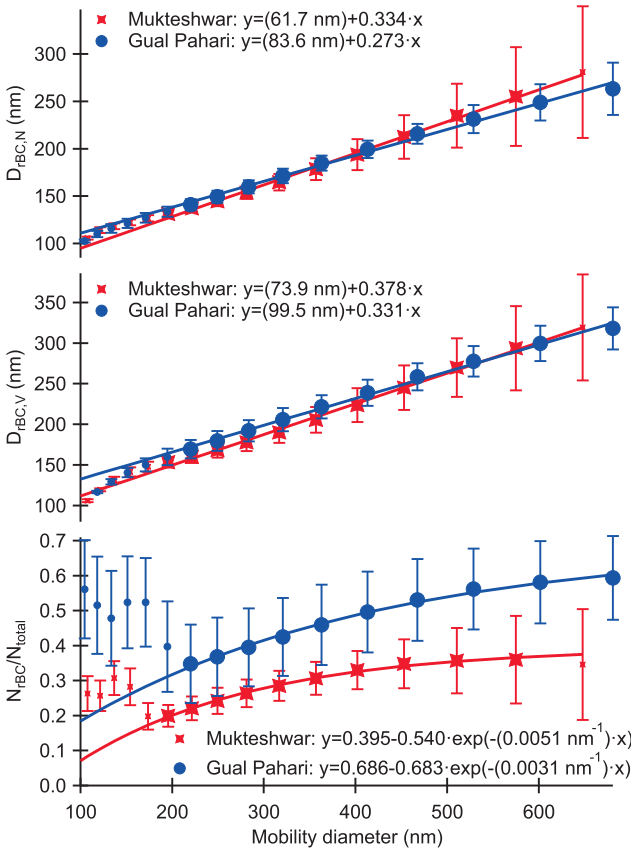

Figure 5. Size dependent rBC mixing state parameters for Gual Pahari and Mukteshwar. The upper panel shows the number mean rBC core volume equivalent diameters and the mid panel shows those based on the rBC volume. The lower panel shows rBC particle number fractions. Solid lines are the fits to the data (ignoring bad data points indicated by the smaller marker size). Error bars indicate ± 1 standard deviation limits.

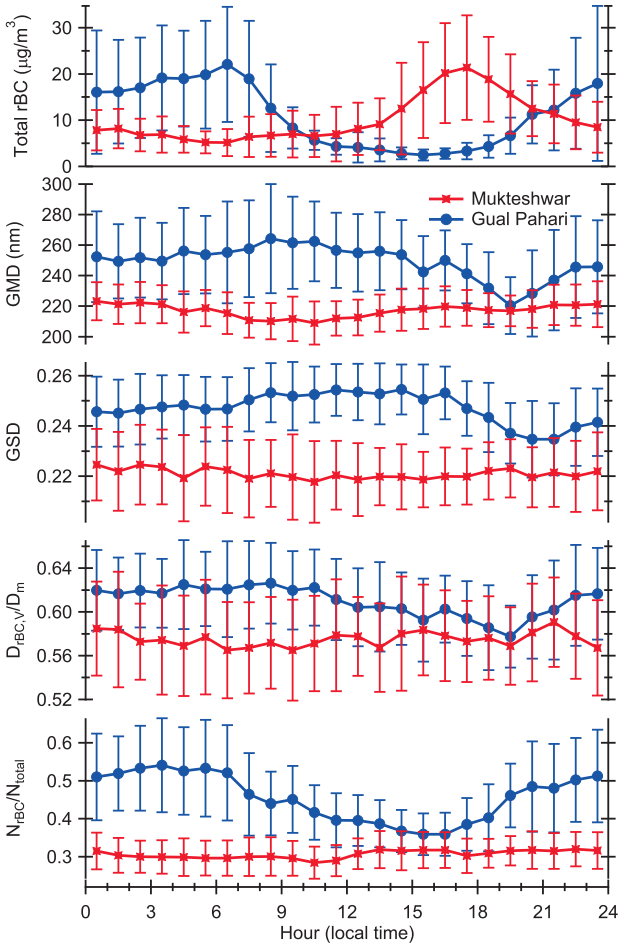

Figure 6. Diurnal cycles of rBC core mass size distribution parameters (total mass concentrations and geometric mass mean diameter and standard deviation), rBC core to mobility diameter ratios and fractions of particles containing rBC. The diameter ratios and fractions are calculated for the 360 nm mobility size. Error bars indicate ±1 standard deviation limits. Mukteshwar total rBC mass concentration and its standard deviation have been multiplied by a factor of ten.

Deleted:

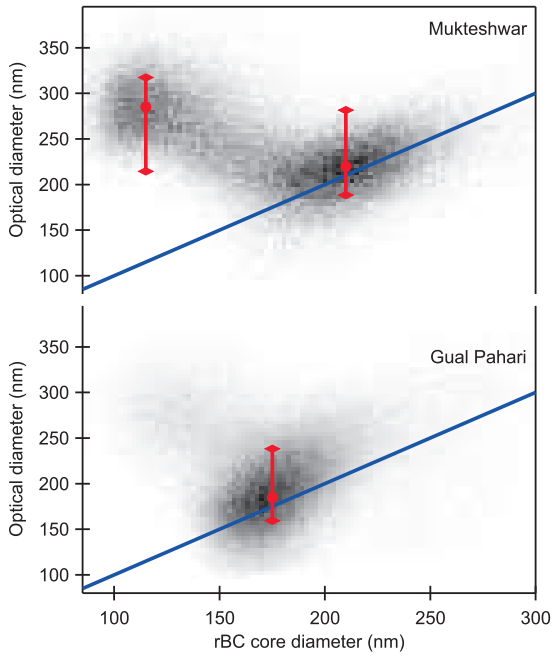

New:

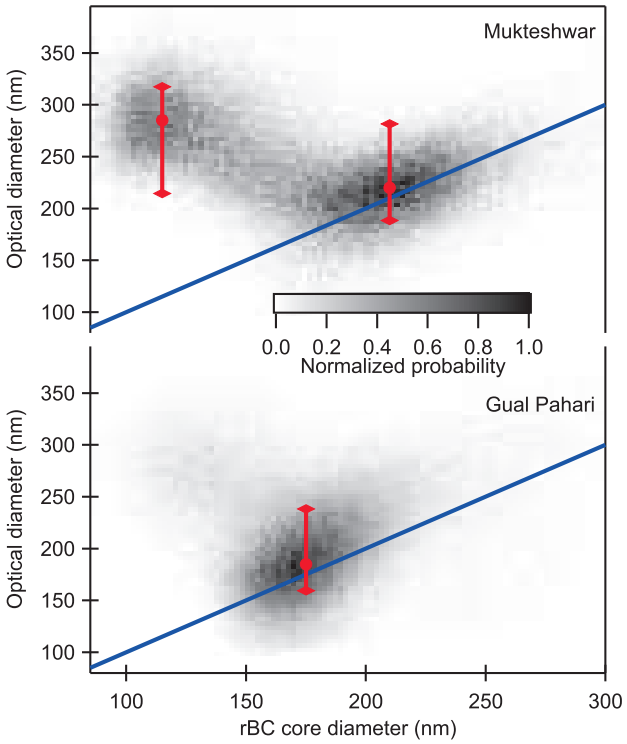

Figure 7. Distributions of single particle optical and rBC core diameters for the 360 nm mobility size and 30–35 °C instrument temperature range (~~darker color indicates higher probability~~probabilities normalized by the maximum values). The blue lines indicate equal rBC and optical diameters. The red markers represent the mode center points and the error bars are based on calculations using different optical constants (ammonium sulfate and rBC).